INSTITUT DE FRANCE
Académie des sciences

# Comptes Rendus

# Chimie

Zhixin Li, Qinhui Wang, Yi Feng and Mengxiang Fang

**Experiments and DFT study on modified CaO-based adsorbents for enhanced $CO_2$ capture**

Volume 24, issue 2 (2021), p. 177-187

Published online: 6 May 2021

https://doi.org/10.5802/crchim.79



*Les* Comptes Rendus. Chimie *sont membres du*
*Centre Mersenne pour l'édition scientifique ouverte*
www.centre-mersenne.org
e-ISSN : 1878-1543

*Comptes Rendus*
*Chimie*
**2021**, 24, nº 2, p. 177-187
https://doi.org/10.5802/crchim.79

Full paper / *Article*

# Experiments and DFT study on modified CaO-based adsorbents for enhanced $CO_2$ capture

**Zhixin Li[a], Qinhui Wang*, [a], Yi Feng[a] and Mengxiang Fang[a]**

[a] State Key Laboratory of Clean Energy Utilization, Zhejiang University, Hangzhou, Zhejiang 310063, China

*E-mails:* lzx196971@163.com (Z. Li), qhwang@zju.edu.cn (Q. Wang), 21427124@zju.edu.cn (Y. Feng), mxfang@zju.edu.cn (M. Fang)

**Abstract.** CaO-based adsorbents for carbon capture represent a promising technology for reducing carbon emission. In this study, we prepare metal oxide-doped multifarious CaO-based adsorbents using the hydration method. We investigate the effect of various working conditions, such as temperature and carbonation time, on different adsorbents in a fixed-bed reactor under multiple carbonation–calcination cycles. We examine the behavior of different metal oxides-doped synthetic adsorbents using density functional theory calculation based on experiments. The results prove that 5 wt% $ZrO_2$-doped adsorbents show excellent $CO_2$ adsorption efficiency, which reaches up to 38.4% after 20 carbonation–calcination cycles at 700 °C with 15 vol% $CO_2$. The adsorbents doped with other metal oxides are also useful for $CO_2$ capture to varying degrees. The adsorption energy of $CO_2$ molecules on modifiequationed adsorbents is higher than that on pure CaO, especially for Zr, where the adsorption energy reached 2.37 eV. The calculation results are in good agreement with the experimental data.

**Keywords.** Density functional theory, CaO-based adsorbents, Carbon capture, Carbonation–calcination cycles, Adsorption energy.

*Manuscript received 23rd August 2020, revised 23rd September 2020 and 29th March 2021, accepted 1st April 2021.*

## 1. Introduction

Fossil fuels are essential to modern society, as they are one of the most important contributors to world's energy consumption. However, their excessive use is leading to a sharp increase in $CO_2$ emissions, which creates many environmental concerns, such as the "greenhouse effect". Statistical data show that carbon emissions of China increased by around 6 billion tons from 2001 to 2017. In 2016, China became the world's largest emitter of greenhouse gases [1], so reducing carbon dioxide emissions is a challenging problem for China. A CaO-based carbon capture technology is considered promising for carbon emission reduction, and hence it is studied here in detail. The circulatory system contains a reactor to capture $CO_2$ and a calcination furnace for regenerating CaO-based adsorbents [2–4]. However, calcination may also bring about deformation and sintering of particles of the adsorbent [5,6]. After multiple carbonation–calcination cycles, the adsorption effequationiciency of calcium-based adsorbents decreased significantly [7,8].

* Corresponding author.

Calcium-based adsorbents have been modified using different methods: addition of other metal elements, changing the preparation methods, optimizing reaction conditions [9–12]. Lee *et al.* [13] prepared an innovative, calcium-based adsorbent doped with $Na_2CO_3$ and found that its reaction with $CO_2$ can take place at a lower adsorption temperature, thus reducing the energy demand. Pecharaumporn *et al.* [14] studied the performance of a synthetic Al–CaO-based system on $CO_2$ capture and found that synthetic adsorbents with gluconic acid as precursor display a good adsorption capacity. Guo *et al.* [15] demonstrated the role of microstructure and oxygen vacancy (Zr–Ce) in $CO_2$ adsorption and discovered that the synthetic adsorbent guaranteed good $CO_2$ capture ability when the ratios Ca/Zr/Ce were 30:0.5:0.5 even after 35 carbonation–calcination cycles. Yoon *et al.* [16] added $ZrO_2$ in CaO adsorbents using the sol–gel method to prepare a new adsorbent and obtained a $CO_2$ adsorption capacity around 77.3 wt% (17.6 mol/kg). Tong *et al.* [17] proposed a semi-industrial process for preparing calcium-based adsorbent pellets and demonstrated that the microsphere adsorbent containing 5 wt% uric acid had the best $CO_2$ adsorption capacity. Wang *et al.* [18] manufactured stable Al–CaO-based adsorbents with different mass ratios using hydration, co-precipitation, and sol–gel spontaneous combustion and found that the preparation method had a significant impact on the structure of the synthesized adsorbents. Antzara *et al.* [19] investigated the behavior of CaO adsorbents containing $ZrO_2$ using a fluidized-bed reactor and found that the deactivation rate of adsorbents was 16% lower after 20 carbonation–calcination cycles. Qin *et al.* [20] used a chemical combustion chain toequation provide the energy demand of regeneration of CaO particles and indicated that increasing water vapor pressure could significantly reduce the reaction deactivation rate of CaO/CuO sorbents in the Ca–Cu complex chemical circulation.

To further investigate the adsorption mechanism of CaO-based adsorbents, density functional theory (DFT) calculations have been widely used to study carbon capture [21–24]. Ma *et al.* [25] investigated the reaction between CaO/$Ca_{12}Al_{14}O_{33}$ adsorbent and $CO_2$ in the presence of water vapor and proved that DFT calculations accurately predicted the adsorption results of CaO-based sorbents under different reaction atmospheres. Liu *et al.* [26] added different metal elements to calcium sorbents to study the adsorption performance and found that addition of Zr effectively improved the adsorption ability of CaO-based adsorbents. Fan *et al.* [27] analyzed the properties of a pressurized calcium-based adsorbent with steam in a spout-fluidized-bed reactor and reported that steam may have little catalytic effect on the carbonation of adsorbents. Guo *et al.* [28] studied the effect of $Mg^{2+}$ in the CaO lattice for $CO_2$ capture at high temperature. Further results showed that there was a strong adsorption effect between the $CO_2$ molecule and $O^{2-}$. Jensen *et al.* [29] studied the adsorption of $CO_2$ on MgO and CaO by quantum chemical calculations and compared the data with the infrared spectra in the literature. Dai *et al.* [30] examined the behavior of $H_2O$ molecules on the surface of CaO (100). The results of the adsorption energy calculations proved that the interaction between $H_2O$ and CaO were due to chemical adsorption. Xu *et al.* [31] conducted experiments and DFT calculations on the adsorbent doped with different metal oxides. Ma *et al.* [32] synthesized an innovative calcium-based adsorbent with hollow core-shell structure and demonstrated that Al effectively delays the slagging and sintering of the synthetic adsorbent. However, there are only limited studies available on the combination of experiments and DFT calculations for different calcium-based adsorbents, and this has been investigated in the present study.

We have examined CaO-based sorbents containing different metal elements using a hydration method. The performance of the CaO-based adsorbent was tested in a fixed-bed reactor under different working conditions. DFT calculations were used to determine the key parameters of different adsorbents, which can help explain the experimental results.

## 2. Experimental part

### 2.1. *Materials*

Modified CaO-based adsorbents were prepared using the hydration method. Analytical reagent (AR)-grade CaO particles were used for the experiment. Other materials included $ZrO_2$ (99%), 200–300-mesh $Al_2O_3$, and CuO (99%). Five adsorbent samples doped with metal oxides were prepared: (1) 95 wt% CaO + 5 wt% $ZrO_2$; (2) 95 wt% CaO + 5 wt% $Al_2O_3$; (3) 95 wt% CaO

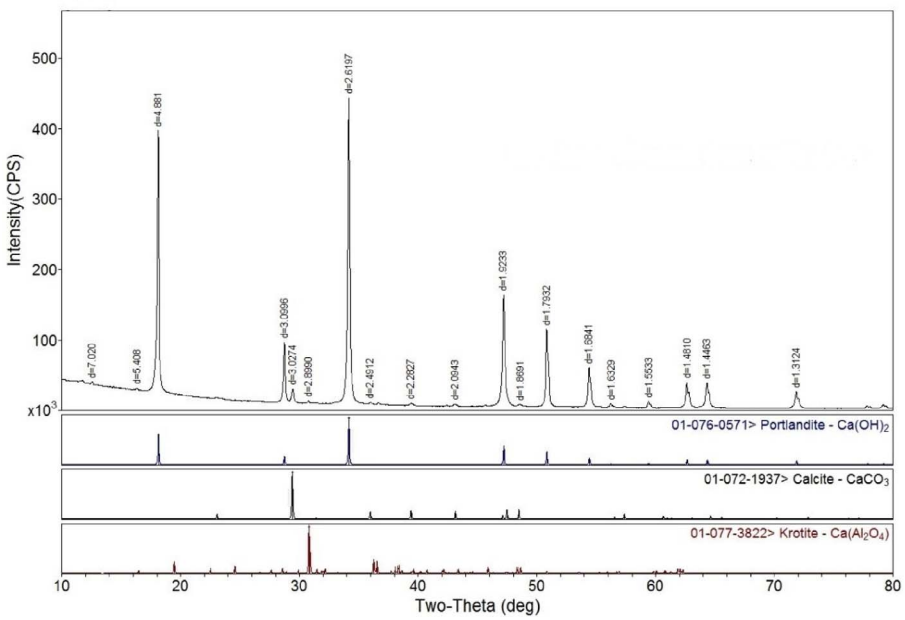


**Figure 1.** XRD spectrum of $Al_2O_3$-doped sample. Lower tracks show spectra for $Ca(OH)_2$, $CaCO_3$ and $Ca(Al_2O_4)$ for comparison.

+ 2.5 wt% $ZrO_2$ + 2.5 wt% $Al_2O_3$; (4) 95 wt% CaO + 5 wt% CuO; (5) 100 wt% CaO. All samples were evenly stirred in deionized water. After allowing samples to stand for 30 min, a specimen was put into an oven and dried for 12 h at 100 °C, and particles with diameter of 200 μm were chosen for experiment. X-ray diffraction (XRD) shows essentially the same main $Ca(OH)_2$ and secondary $CaCO_3$ peaks for all 5 samples (Figure 1 shows a typical spectrum obtained with the $Al_2O_3$-doped sample). Due to moisture remaining after drying, CaO particles reacted with $H_2O$ to form $Ca(OH)_2$; then a small amount of $Ca(OH)_2$ and $CO_2$ reacted to form $CaCO_3$. Therefore, samples were subsequently calcined for 3 h at 900 °C to remove $Ca(OH)_2$ and $CaCO_3$.

## 2.2. *Experimental apparatus*

We used a fixed-bed reactor in our experiments. The outer and inner diameters of the quartz tube were 125 and 120 mm, respectively, and its length was 1400 mm. The samples were placed in a quartz boat and gently pushed to the center of the quartz tube. The heating and cooling rates were set at 15 and 20 °C/min, respectively. The carbonation reaction temperature varied from 600 to 750 °C, depending on the working condition, and the calcination temperature was set at 850 °C. The reaction time for carbonation and calcination was set at 25 and 15 min, respectively. Here, 500 mg of experimental samples was investigated for 20 carbonation–calcination cycles under various working conditions.

The $CO_2$ and $N_2$ gas valves were connected to the fixed-bed reactor. The total gas flow was fixed at 400 ml/min. The purge and furnace gases composed of $N_2$ were used to effectively preserve the fixed-bed reactor. The carbonation conversion rate of the synthetic adsorbent was defined as

$$X = \frac{M_t - M_0}{M_0 f} \times \frac{M_{\mathrm{CaO}}}{M_{\mathrm{CO_2}}}, \tag{1}$$

where $M_t$ is the weight of the adsorbent at time $t$, $M_0$ is the original mass of the adsorbent after calcination, $f$ is the mass fraction of CaO in the adsorbent, $M_{\mathrm{CO_2}}$ and $M_{\mathrm{CaO}}$ are the molar masses of $CO_2$ and CaO, respectively, and $X$ is the carbonation conversion after multiple carbonation–calcination cycles.

The XRD analysis was carried out to study the specific distribution of crystal phase in the sample. To determine the crystal structure, atomic coordinates, and absolute configuration, we used a Gemini

XRD analyzer, with a CCD detector and a cryogenic system.

### 2.3. *Preparation of DFT calculation*

We established the crystal structure model using Materials Studio software to perform the calculation. The CaO crystal has a cubic structure. The lattice constant after optimization is 4.862 Å, which is in agreement with the experimental results [33]. The C–O bond length and O–C–O bond angle of the $CO_2$ cell are 1.173 Å and 179.895°, respectively, which is consistent with the experimental results [34]. The CaO crystal cell is defined by adopting crystal indices (100). A vacuum layer with a thickness of 15 Å is chosen. Simultaneously, the CaO (110) surface is modified by adding Zr, Al, and Cu to achieve the doping of metal elements and structure optimization.

Calculations were performed using the general gradient approximation method and the Cambridge Serial Total Energy Package (CASTEP) module. The cut-off energy value of 570 eV was selected for truncation. The energy difference between adjacent ion steps was less than $1.0 \times 10^{-5}$ eV/atom. The maximum atomic interaction force, maximum atomic stress, and atomic displacement were 0.3 eV/nm, 0.05 GPa, and 0.0001 nm, respectively. Here, the energy convergence standard of the electron step in the self-consistent field operation was $10^{-5}$ eV/atom. The $K$ point was set as $3 \times 4 \times 1$ to ensure the accuracy of calculation. The adsorption energy $E_{ad}$ is defined as

$$E_{ad} = E_{system} - (E_{adsorb} + E_{substrate}), \qquad (2)$$

where $E_{system}$, $E_{adsorb}$, and $E_{substrate}$ are the total electronic energy of the system after adsorption, the electronic energy of the adsorbate, and the electronic energy of the surface, respectively.

## 3. Results and discussion

### 3.1. *Performance test of modified adsorbents*

#### 3.1.1. *Adsorption properties of different modified CaO-based adsorbents*

We evaluated the performance of modified adsorbents after multiple carbonation–calcination cycles. During the experiment, $N_2/CO_2$ and $N_2$, respectively, were the carbonation and calcination atmospheres. Figures 2 and 3 show the experimental results of the adsorption efficiency of adsorbents after 20 carbonation–calcination cycles at 700 and 650 °C, respectively, at 15 vol% $CO_2$ concentration. The adsorption efficiency of all adsorbents at 700 °C was higher than that at 650 °C, which indicated that the increase in temperature was beneficial to the adsorption reaction. When the carbonation temperature was 700 °C, the initial efficiency of the adsorbent with 5 wt% $ZrO_2$ was 72%. After 16 carbonation–calcination cycles, the adsorption efficiency ap-

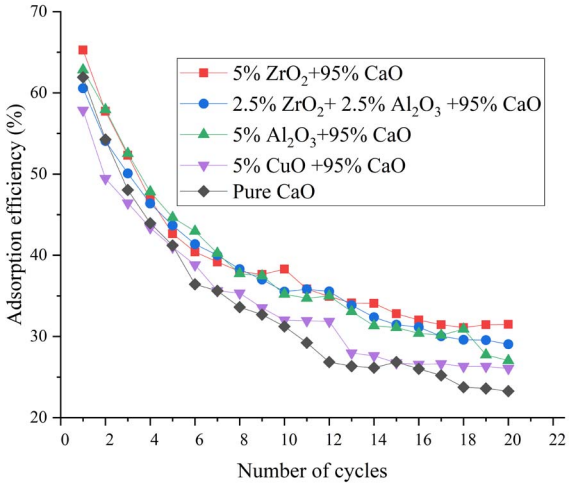


**Figure 2.** Adsorption efficiency of different modified CaO-based adsorbents at 650 °C.

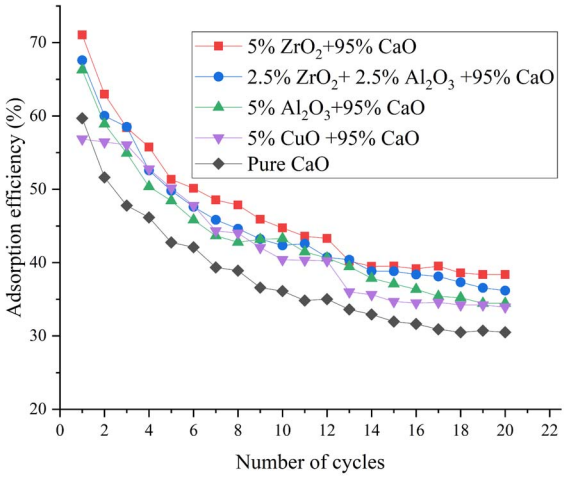


**Figure 3.** Adsorption efficiency of different modified CaO-based adsorbents at 700 °C.

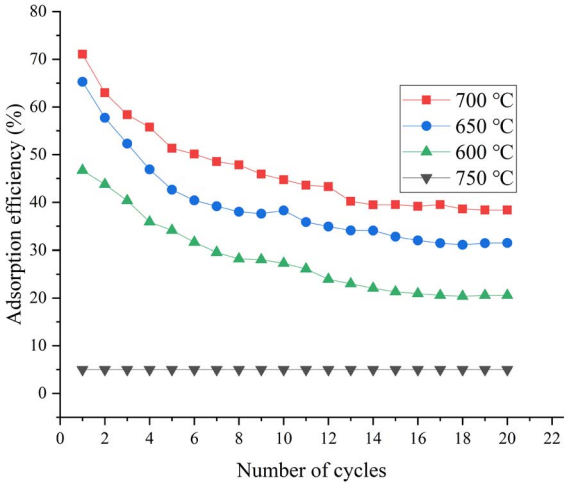


**Figure 4.** Effect of temperature on CaO-based adsorbents doped with 5% $ZrO_2$.

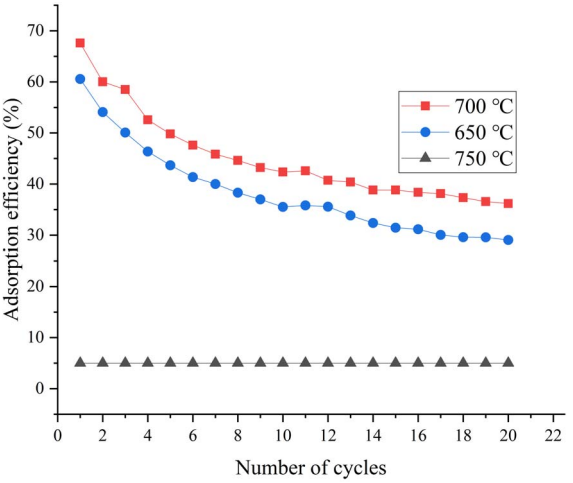


**Figure 5.** Effect of temperature on CaO-based adsorbents doped with 2.5% $ZrO_2$ + 2.5% $Al_2O_3$.

peared to be stable at 38.4%, which represented an increase of approximately 9.4% compared with a pure CaO adsorbent. The adsorption efficiency of adsorbents doped with $Al_2O_3$ and CuO after 20 cycles was 34.5% and 34%, respectively. It should be pointed out that the adsorption capacity of CaO-based adsorbent doped with Cu decreased significantly during the 12–13 carbonation–calcination cycles. The adsorbent was inactivated due to fusion at high calcination temperature. However, lower

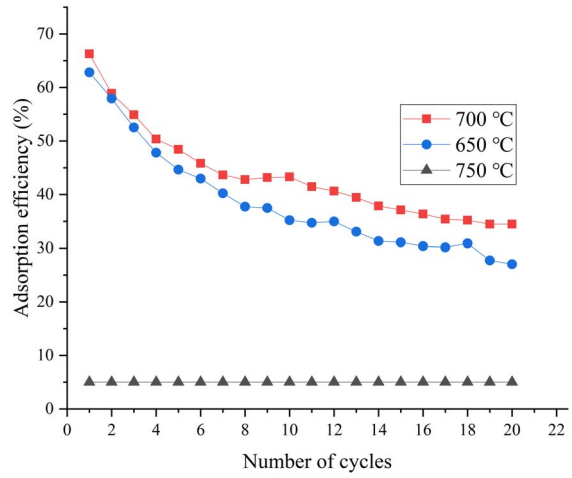


**Figure 6.** Effect of temperature on CaO-based adsorbents doped with 5% $Al_2O_3$.

calcination temperature also guaranteed that the adsorbent with Cu showed a good carbon capture capability. Overall, the adsorbent doping with 5 wt% $ZrO_2$ demonstrated the strongest anti-sintering ability and the best adsorption ability.

#### 3.1.2. *Effect of carbonation temperature on the performance of modified adsorbents*

We also investigated the performance of modified adsorbents at different carbonation temperatures. The adsorption efficiency of adsorbents doped with (a) 5 wt% $ZrO_2$, (b) 2.5 wt% $ZrO_2$ + 2.5 wt% $Al_2O_3$, and (c) 5 wt% $Al_2O_3$ increased by (a) 6.9%, (b) 7.15%, and (c) 7.43% when the carbonation temperature increased from 650 to 700 °C (20 carbonation–calcination cycles). The effect of temperature on the performance of adsorbents can also be clearly seen in Figures 4–6. However, adsorption efficiency decreased significantly at 750 °C (Figure 7). Figure 8 further confirmed 700 °C as the optimal temperature.

#### 3.1.3. *Effect of carbonation time on the performance of modified adsorbents*

The effect of carbonation time on the adsorption efficiency of adsorbents was also investigated. The 2.5 wt% $Al_2O_3$ + 2.5 wt% $ZrO_2$ adsorbent was our main object of study. The carbonation temperature was 700 °C, and the atmosphere was $N_2/CO_2$ with 15% $CO_2$ concentration. As shown in Figures 9 and 10, the adsorption efficiency increased by 23.2%,

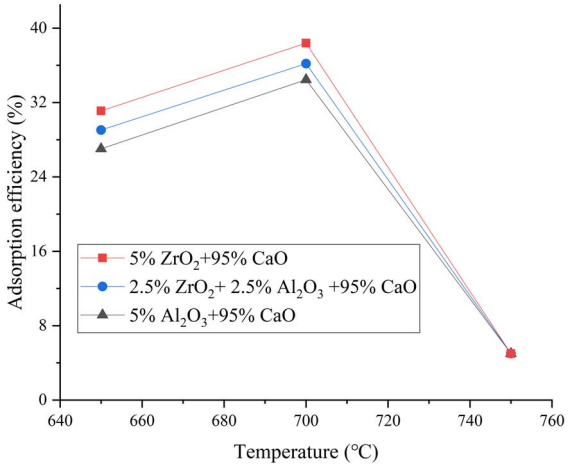


**Figure 7.** Effect of temperature on modified CaO-based adsorbents after 20 cycles.

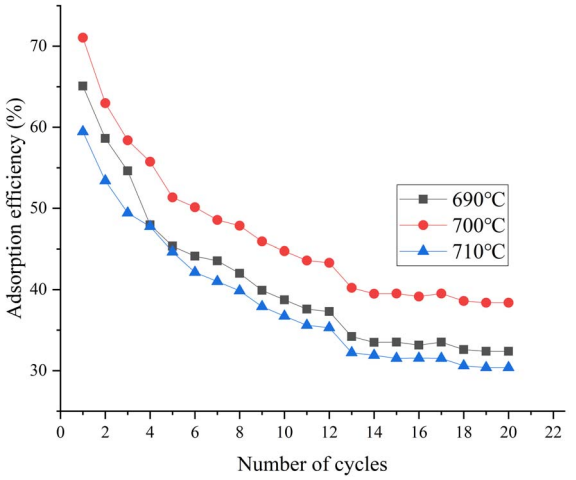


**Figure 8.** Optimal adsorption temperature of CaO-based adsorbents doped with 2.5% $ZrO_2$ + 2.5% $Al_2O_3$.

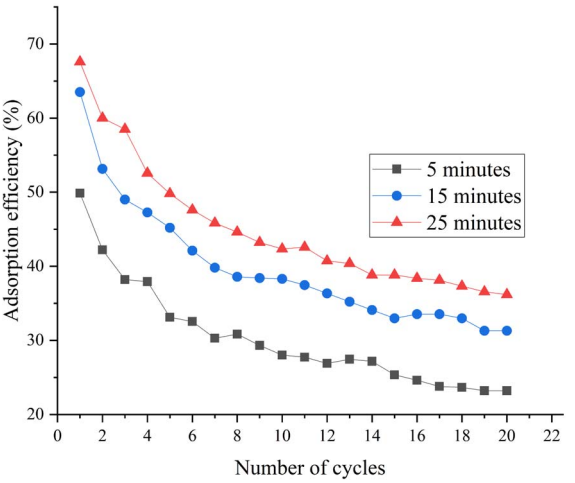


**Figure 9.** Effect of carbonation time on CaO-based adsorbents doped with 2.5% $ZrO_2$ + 2.5% $Al_2O_3$.

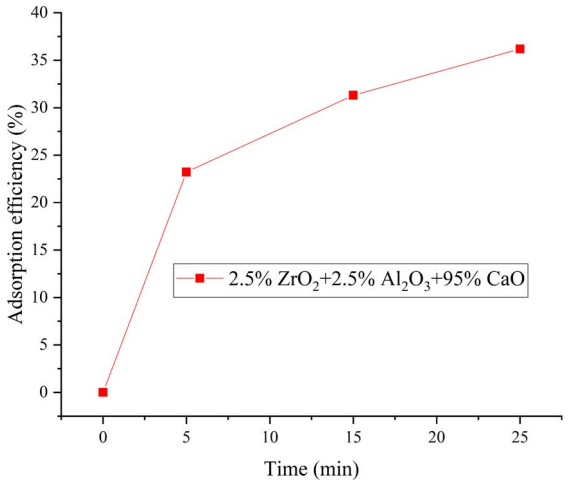


**Figure 10.** Adsorption reaction analysis of CaO-based adsorbents doped with 2.5% $ZrO_2$ + 2.5% $Al_2O_3$ after 20 carbonation–calcination cycles.

8.2%, and 4.7% for 0–5 min, 5–15 min, 15–25 min, respectively. The initial steepness of the curve in Figure 10 shows that the carbonation reaction was very fast between 0–5 min. Between 5 and 15 min (the transition period), the adsorption efficiency of adsorbents increased relatively rapidly. However, the adsorption reaction became slow between 15 and 25 min (reaction diffusion stage). In particular, the 0–5 min rapid stage of carbonation ensured good $CO_2$ capture capacity.

### 3.1.4. *Effect of $CO_2$ concentration on the performance of modified adsorbents*

We also studied the effect of $CO_2$ concentration on the adsorption performance of modified adsorbents. A CaO-based adsorbent doped with 5 wt% $ZrO_2$ was set as the main object of study. Although the volume fraction of $CO_2$ in coal-fired flue gas was about

15%, it was imperative to study the $CO_2$ concentration higher than 15% in order to determine the performance of adsorbents more clearly. The adsorption efficiency of adsorbents was investigated under increasing carbonation–calcination cycles with 40, 15, and 8 vol% $CO_2$. The working conditions in the calcination stage were the same in all experiments. Figure 11 shows that the adsorption efficiency of adsorbents was nearly uniform under 40% and 15% $CO_2$ but decreased sharply with 8% $CO_2$. Figure 12 demonstrates that the efficiency was consistent during the first cycle. However, after 20 carbonation–calcination cycles, the adsorption efficiency of adsorbents with 40 vol% $CO_2$ concentration was higher by approximately 9.5% than with 15 vol% $CO_2$.

This phenomenon was explained as follows. First, the whole carbonation reaction process was divided into two stages: the rapid reaction stage and the reaction diffusion stage. Thereafter, the $CO_2$ diffusion rate in the carbonation stage was determined by temperature and $CO_2$ concentration. In addition, the sintering degree was based on the same calcination temperature and time for all adsorbents. Figures 11 and 12 suggest that the $CO_2$ diffusion rate is mainly depended on $CO_2$ concentration at 650 °C, but determined by temperature and $CO_2$ concentration together at 700 °C. The diffusion rates with 40 and 15 vol% $CO_2$ are similar at 650 °C (both curves essentially overlap). The diffusion rate with 8 vol% $CO_2$ was far slower than that under high $CO_2$ concentration, which led to the sharp decrease in adsorption efficiency.

Figure 12 shows that the diffusion rate of the $CO_2$ molecule was rapid with 40 vol% $CO_2$ concentration at 700 °C, so the adsorption efficiency of adsorbents in rapid reaction stage was also higher. However, the $CO_2$ molecular diffusion rate with 15 vol% $CO_2$ was relatively slow, and the $CaCO_3$ produced in the rapid reaction stage might result in pore blockage, which would ultimately reduce the adsorption efficiency.

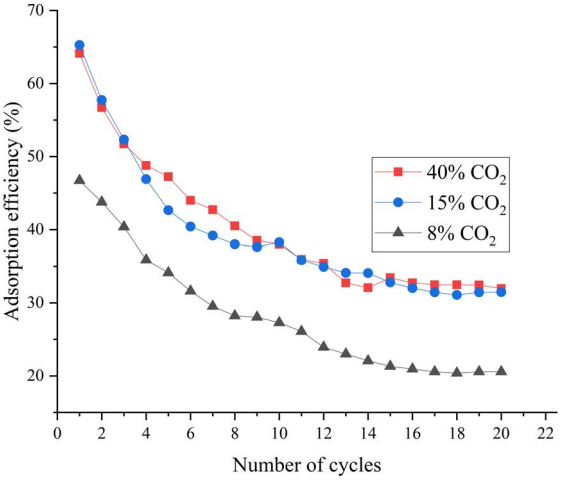


**Figure 11.** Effect of $CO_2$ concentration on CaO-based adsorbents doped with 5% $ZrO_2$ at 650 °C.

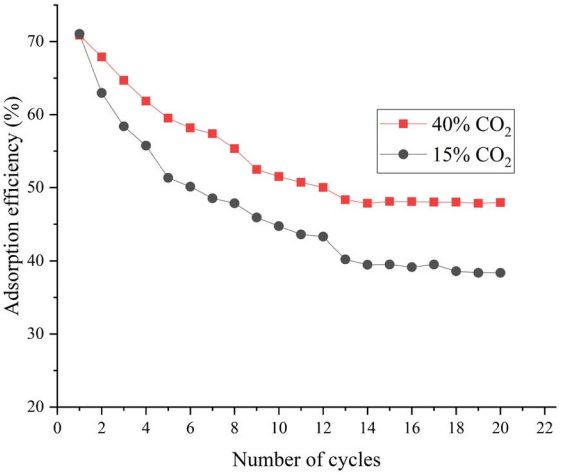


**Figure 12.** Effect of $CO_2$ concentration on CaO-based adsorbents doped with 5% $ZrO_2$ at 700 °C.

### 3.2. *Results of DFT calculation*

To verify the experimental results for adsorbents under various working conditions, DFT calculations were performed using MS software. The carbonation reaction between CaO-based adsorbents doped with different metals and $CO_2$ molecules was studied in detail. The structure of $CO_2$ molecules and CaO cells has been calculated before [25,35]. However, in this study, the adsorption reaction between CaO-based adsorbents and $CO_2$ was emphasized. Figure 13 shows the adsorption models of $CO_2$ molecules on the CaO-based adsorbents doped with different metal elements. It could be seen that CaO (110) crystal cells had multiple adsorption sites, including O-top, Ca-top, bridge, and hollow sites. We found that the possibility of forming an anionic carbonate-like $CO_3^{2-}$ structure was high for $CO_2$ molecules on the

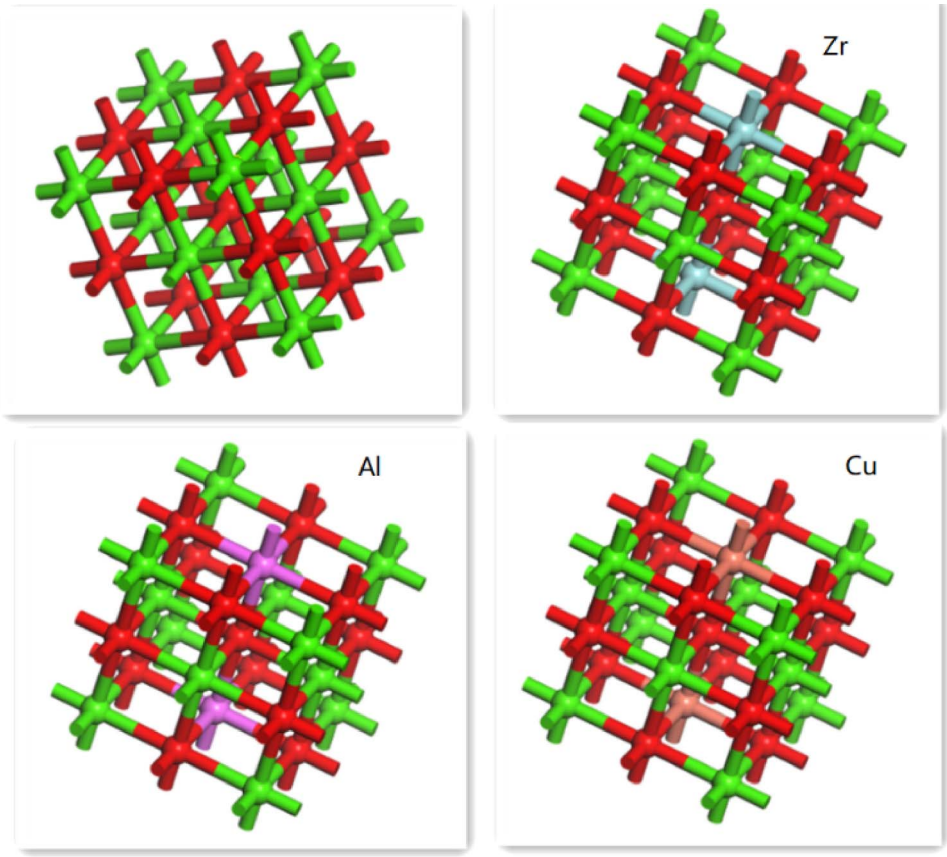


**Figure 13.** Adsorption model of different modified CaO-based adsorbents.

**Table 1.** Main results of DFT calculation

| | CaO (100) | Al–CaO (110) | Zr–CaO (110) | Cu–CaO (110) |
|---|---|---|---|---|
| Ca–O bond angle/° | 90 | 82.74 | 73.4 | 83.587 |
| C–O bond length/Å | 2.9 | 2.796 | 2.329 | 1.506 |
| O–C–O bond angle/° | 141.1 | 142.6 | 119.05 | 132.76 |
| O–C–O bond length/Å | 1.208 | 1.176 | 1.3 | 1.24 |
| $E_{ad}$/eV | 1.715 | 1.98 | 2.37 | 1.81 |

O-top site compared with other adsorption sites. Other studies showed that $CO_2$ molecules were also inclined to be adsorbed at the O-top position [26]. Therefore, we only investigated the adsorption conditions at the O-top site. The adsorption results are given in Table 1, including adsorption energy and bond length angle. The adsorption energy of pure CaO was 1.715 eV. The structure of the CaO crystal cell changed slightly upon $CO_2$ adsorption, the Ca–O bond angle remained 90°. The C–O bond length was 2.9 Å, and the bond angle of the $CO_2$ molecule was 141.1°.

The results show that the adsorption energy of $CO_2$ molecules is higher with metal-doped CaO-based adsorbents, especially for Zr. The higher adsorption energy ensured that the C–O bond was more stable, and the adsorbents had much stronger ability to resist sintering. Figures 14–17 show the

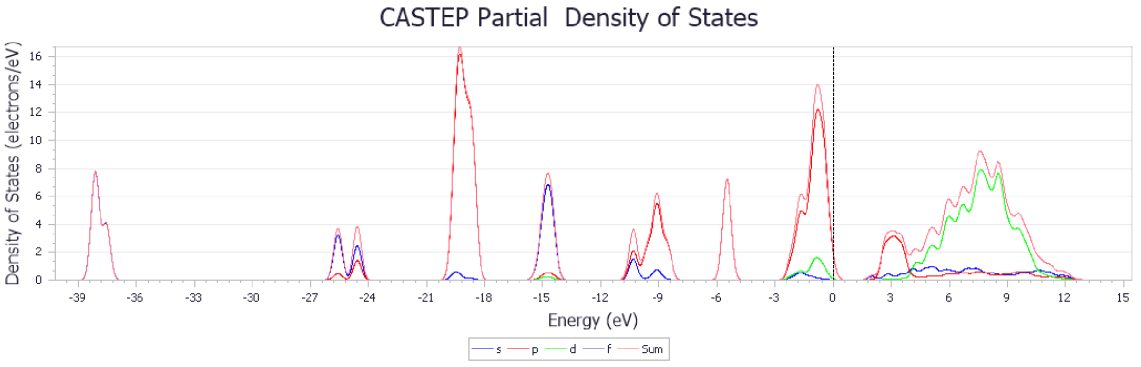


**Figure 14.** PDOS of CaO adsorbent.

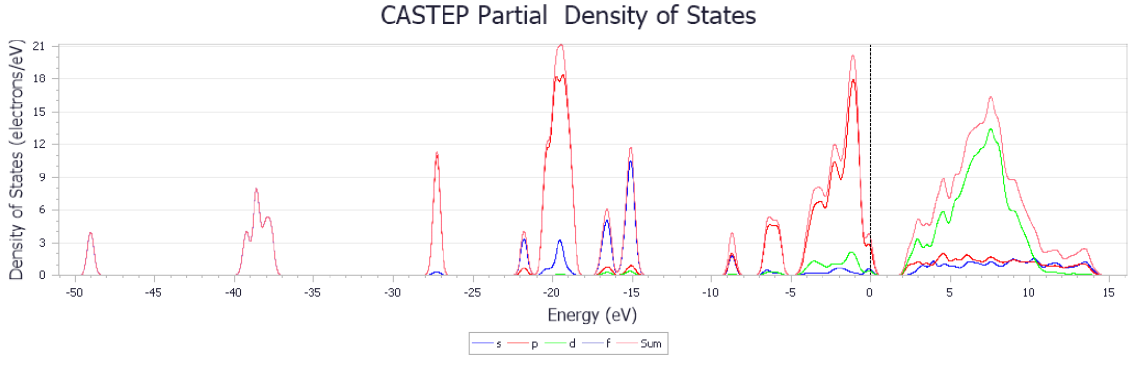


**Figure 15.** PDOS of CaO-based adsorbent doped with $ZrO_2$.

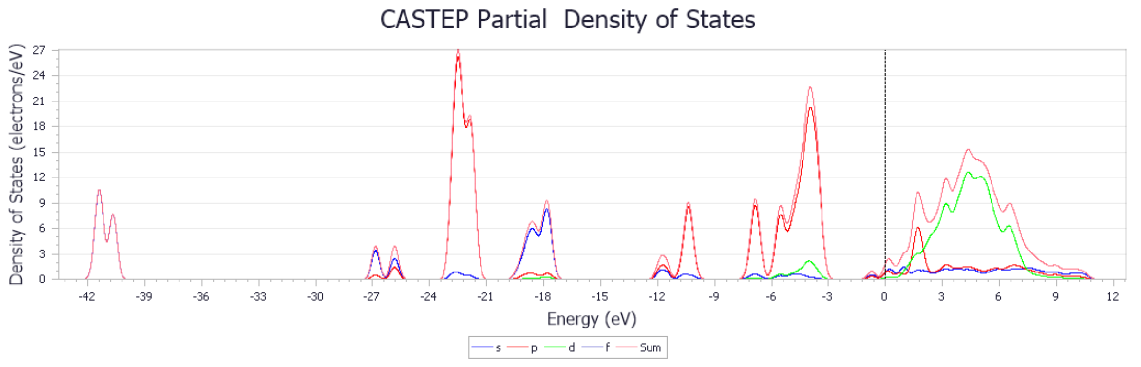


**Figure 16.** PDOS of CaO-based adsorbent doped with $Al_2O_3$.

changes in energy band structure of different modified CaO-based adsorbents after adsorption reaction. In summary, the partial density of state of CaO-based adsorbents doped with different metal elements was shifted from right to left. In particular, when the peak height of the waveform in figures is large, then the degree of hybridization between different atoms is higher.

Figure 15 shows the best adsorption performance compared with other results. It was found that the

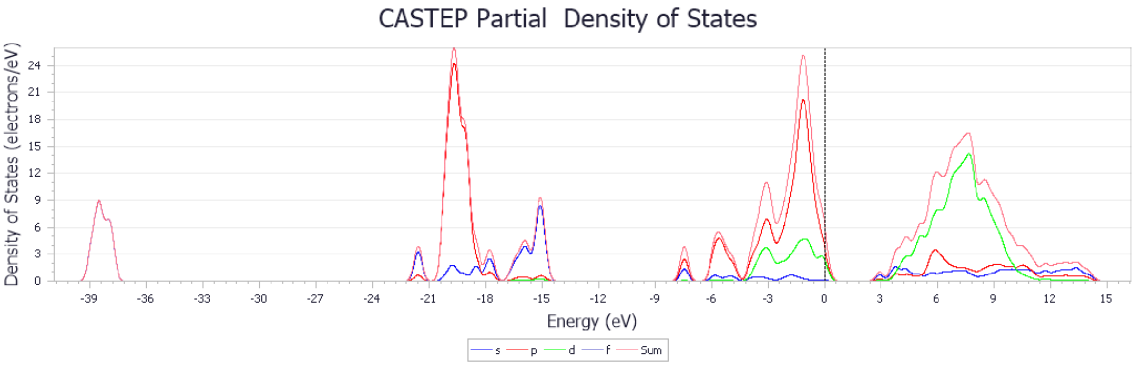


**Figure 17.** PDOS of CaO-based adsorbent doped with CuO.

structure in $CO_2$ molecules and CaO crystal cells had also changed and the O–C–O bond angle got smaller, which was caused by the deformation in electrons from the $O^{2-}$ transferred to the C atom. It should be noted that there was no obvious change in the energy band structure of Cu-doped adsorbent, although some researchers have observed benefits for carbon reduction [20,36–38]. It might be explained that the method was applied for the $CO_2$ catalytic reduction rather than adsorption reaction. The Cu-doped adsorbent may have melted during the experiment at high calcination temperature. The experimental results are consistent with the DFT calculations for all the carbonation temperatures examined here. It was clear that the Zr-doped adsorbent had the best adsorption efficiency after 20 carbonation–calcination cycles.

## 4. Conclusions

In this study, CaO-based adsorbents doped with different metal oxides were prepared using the hydration method. The performance of the modified adsorbents under various working conditions was studied and the results show that the modified calcium-based adsorbent doped with 5 wt% $ZrO_2$ has excellent $CO_2$ adsorption capacity. The adsorption efficiency is around 38.4% after 20 carbonation–calcination cycles for a carbonation temperature of 700 °C and 15 vol% $CO_2$, which is 9.4% higher than that of the pure CaO adsorbent. The adsorbents doped with other metal oxides demonstrate higher anti-sintering ability under high calcination temperature, which suggests a promising research direction for industrial applications. The effect of carbonation time on adsorption efficiency shows that extending carbonation time enhances $CO_2$ capture. In addition, the reaction model for modified adsorbents was established by DFT calculation to further explain the experimental results. The results indicate that the adsorption energy of adsorbents doped with metal oxides is higher than that of pure CaO, and the values are 2.37 eV for $ZrO_2$–CaO, 1.98 eV for $Al_2O_3$–CaO, 1.81 eV for CuO–CaO, and 1.715 eV for pure CaO, respectively. The maximum adsorption energy of the adsorbent doped with 5 wt% $ZrO_2$ is 2.37 eV. The greater adsorption energy is favorable to strengthen the anti-sintering ability of adsorbents, so the theoretical results of DFT calculation are consistent with the experimental results.

## Acknowledgment

This work was supported by The National Key Research and Development Program of China (No. 2019YFE0100100-05).

## References

[1] Y. Zhang, S. Li, T. Luo, J. Gao, *J. Clean. Product.*, 2020, **265**, article no. 121843.
[2] H. Li, M. Qu, Y. Yang, Y. Hu, W. Liu, *Chem. Eng. J.*, 2019, **374**, 619-625.
[3] Y. Zhang, X. Gong, X. Chen, L. Yin, J. Zhang, W. Liu, *Fuel*, 2018, **232**, 205-214.
[4] S. He, Y. Hu, T. Hu, A. Ma, Q. Jia, H. Su, S. Shan, *J. Alloys Comp.*, 2017, **701**, 828-833.
[5] X. Gong, Z. Wang, Z. Wang, J. Cao, S. Zhang, *Powder Technol.*, 2018, **336**, 92-101.

[6] H. Sun, C. Wu, B. Shen, X. Zhang, Y. Zhang, J. Huang, *Mater. Today Sustain.*, 2018, **1–2**, 1-27.
[7] J. M. Valverde, P. E. Sanchez-Jimenez, L. A. Perez-Maqueda, *Appl. Energy*, 2014, **126**, 161-171.
[8] X. Liu, X. Ma, L. He, S. Xu, *Chin. J. Chem. Eng.*, 2017, **25**, 1412-1421.
[9] Y. Hu, H. Lu, W. Liu, Y. Yang, H. Li, *Chem. Eng. J.*, 2020, **396**, article no. 125253.
[10] S. Scaccia, G. Vanga, D. M. Gattia, S. Stendardo, *J. Alloys Compounds*, 2019, **801**, 123-129.
[11] Q. Hu, C. H. Wang, *Bioresour. Technol.*, 2020, **310**, article no. 123384.
[12] H. Wang, Z. Li, N. Cai, *Chem. Eng. J.*, 2020, **394**, article no. 124892.
[13] C. H. Lee, S. W. Choi, H. J. Yoon, H. J. Kwon, H. C. Lee, S. G. Jeon, K. B. Lee, *Chem. Eng. J.*, 2018, **352**, 103-109.
[14] P. Pecharaumporn, S. Wongsakulphasatch, T. Glinrun, A. Maneedaeng, Z. Hassan, S. Assabumrungrat, *Int. J. Hydrog. Energy*, 2019, **44**, 20663-20677.
[15] H. Guo, J. Feng, Y. Zhao, S. Wang, X. Ma, *J. $CO_2$ Util.*, 2017, **19**, 165-176.
[16] H. J. Yoon, K. B. Lee, *Chem. Eng. J.*, 2019, **355**, 850-857.
[17] X. Tong, W. Liu, Y. Yang, J. Sun, Y. Hu, H. Chen, Q. Li, *Fuel Process. Technol.*, 2019, **193**, 149-158.
[18] N. Wang, Y. Feng, L. Liu, X. Guo, *Fuel Process. Technol.*, 2018, **173**, 276-284.
[19] A. N. Antzara, A. Arregi, E. Heracleous, A. A. Lemonidou, *Chem. Eng. J.*, 2018, **333**, 697-711.
[20] C. Qin, J. Yin, C. Luo, H. An, W. Liu, B. Feng, *Chem. Eng. J.*, 2013, **228**, 75-86.
[21] J. Li, M. Hou, Y. Chen, W. Cen, Y. Chu, S. Yin, *Appl. Surf. Sci.*, 2017, **399**, 420-425.
[22] K. R. Vijisha, M. K, *Int. J. Greenh. Gas Control*, 2017, **58**, 62-70.
[23] M. D. Esrafili, *J. Mol. Graph Model.*, 2019, **90**, 192-198.
[24] M. D. Esrafili, F. Sharifi, L. Dinparast, *J. Mol. Graph Model.*, 2017, **77**, 143-152.
[25] X. Ma, Y. Li, W. Zhang, Z. Wang, J. Zhao, *Chem. Eng. J.*, 2019, **370**, 10-18.
[26] L. Liu, D. Hong, X. Guo, *J. $CO_2$ Util.*, 2017, **22**, 155-163.
[27] Y. Fan, J. G. Yao, Z. Zhang, M. Sceats, Y. Zhuo, L. Li, P. S. Fennell, *Fuel Process. Technol.*, 2018, **169**, 24-41.
[28] H. Guo, Z. Xu, T. Jiang, Y. Zhao, X. Ma, S. Wang, *J. $CO_2$ Util.*, 2020, **37**, 335-345.
[29] B. Jensen, L. Pettersson, *J. Phys. Chem. B*, 2005, **109**, 16774-16781.
[30] W. Dai, Z.-H. Shui, K. Li, *Comput. Theoret. Chem.*, 2011, **967**, 185-190.
[31] Y. Xu, C. Luo, Y. Zheng, H. Ding, Q. Wang, Q. Shen, L. Zhang, *RSC Adv.*, 2016, **6**, 79285-79296.
[32] X. Ma, Y. Li, L. Duan, E. Anthony, H. Liu, *Appl. Energy*, 2018, **225**, 402-412.
[33] P. Yang, L. Duan, H. Tang, T. Cai, Z. Sun, *Greenh. Gases: Sci. Technol.*, 2018, **8**, 1110-1123.
[34] F. Hou, J. Jin, H. Yang, Y. Wang, S. Li, *Appl. Surf. Sci.*, 2019, **475**, 1033-1042.
[35] W. Wang, L. Fan, G. Wang, Y. Li, *Appl. Surf. Sci.*, 2017, **425**, 972-977.
[36] J. Chen, T. Shi, L. Duan, Z. Sun, E. J. Anthony, *Chem. Eng. J.*, 2020, **393**, article no. 124716.
[37] F. N. Ridha, D. Lu, A. Macchi, R. W. Hughes, *Fuel*, 2015, **153**, 202-209.
[38] I. Martínez, J. R. Fernández, J. C. Abanades, M. C. Romano, *Energy*, 2018, **163**, 570-584.